Polyethylene Glycol-Stabilized Gold Nanostars-Loaded Microneedles for Photothermal Therapy of Melanoma

El-Sayed, Nesma; Elbadri, Khalil; Correia, Alexandra; Santos, Hélder A.

Link to publication in University of Groningen/UMCG research database

Polyethylene Glycol-Stabilized Gold Nanostars-Loaded Microneedles for Photothermal Therapy of Melanoma

Nesma El-Sayed,* Khalil Elbadri, Alexandra Correia, and Hélder A. Santos*

Gold nanostars (GNSs) as a photothermal agent have shown great potential for the treatment of cancers like melanoma. Irradiation of the photothermal agents with light of a suitable wavelength generates heat that induces cellular stress and protein denaturation in cancer cells. The delivery of GNSs to skin using fast dissolving microneedles (MNs) presents a promising approach for painless and convenient administration of the therapy. In this study, polyethylene glycol (PEG) stabilized GNSs able to absorb light in the near-infra red region and release heat (up to 65 °C, room temperature) are developed. The cytotoxicity of these nanoparticles is assessed before and after exposure to laser irradiation. GNSs show an instant lethal photothermal effect when tested on B16F10 melanoma cells upon irradiation with 808 nm at a power of 800 mW for 10 min. Loading the GNSs in polyvinylpyrrolidone (PVP) MNs preserves the photothermal effect of GNS and the mechanical properties of MNs. GNS-loaded PVP MNs show efficient piercing in excised porcine skin, fast dissolution in 3 min after insertion and elevation of the skin temperature after laser irradiation (808 nm, 800 mW, 10 min) to 63 °C. Consequently, PEG-stabilized GNSs and PVP MNs are a promising platform for photothermal therapy in melanoma treatment.

1. Introduction

Skin tumors continue to be a lethal problem worldwide, with the increasing rate of superficial skin tumors , especially malignant tumors, such as melanoma, which ranks as the fifth most prevalent cancer type in males, while in females, it occupies the sixth position.[1] Using the traditional treatments represented in surgical removal of the skin tumor and chemotherapy are inconvenient due to the unsatisfying results and the long time required for recovery.

In early-stage melanoma, before metastasis occurrence in lymph nodes, the main treatment for SST is invasive surgery to excise the tumor tissue. However, this usually requires long recovery time with the risk of the tumor relapsing again if the tumor is not eliminated entirely. When removing the tumor tissue, it is recommended to include 9 mm margin for efficient therapy.[2] Therefore, in some critical cases, for example when the tumor occurs on the face or when the tumor occupies large area of the skin, it becomes challenging to fully eliminate the tumor tissue. For advanced melanoma, conventional treatments (i.e., chemotherapies and radiotherapies), can induce systemic toxicity, skin scars in addition to significant probability of the tumor relapsing.[3–5] Alternatively, innovative immunotherapy approaches are being implemented rather than the standard chemotherapy.[6,7] Although immunotherapy has presented high potency, there have been many cases where patients developed drug resistance, and thus, reducing the treatment efficiency. Hence, there is a necessity for further development of various therapeutic strategies of cancer.

Several strategies have been developed for cancer therapy, including photothermal therapy (PPT),[8] photodynamic therapy[9,10] and gas therapy.[11] Photothermal therapy has been

N. El-Sayed, K. Elbadri, A. Correia, H. A. Santos
Drug Research Program
Division of Pharmaceutical Chemistry and Technology
Faculty of Pharmacy
University of Helsinki
Helsinki 00014, Finland
E-mail: nesma.ibrahim@helsinki.fi; h.a.santos@umcg.nl

N. El-Sayed
Department of Pharmaceutics
Faculty of Pharmacy
Alexandria University
Alexandria 21521, Egypt

H. A. Santos
Department of Biomedical Engineering
University Medical Center Groningen
University of Groningen
Ant. Deusinglaan 1, Groningen 9713 AV, The Netherlands

H. A. Santos
W.J. Kolff Institute for Biomedical Engineering and Materials Science
University Medical Center Groningen
University of Groningen
Ant. Deusinglaan 1, Groningen 9713 AV, The Netherlands

recognized to cure subcutaneous cancer, wherein photothermal agents conglomerate within the tumor tissue and generate heat, to kill cancer cells, upon exposure to laser energy. Interestingly, photothermal therapy shows limited resistance and promising therapeutic results.[12] The localized photothermal ablation of the tumor can increase the effectiveness of cancer eradication, while minimizing the side effects.[13,14] Besides, PTT is ideal for superficial tumors due to the ease of accessibility to laser irradiation.

Among several photothermal agents, GNSs have demonstrated a great capacity to generate heat when exposed to near infrared (NIR) irradiation on picosecond timeframe.[15] In addition, their biocompatibility, chemical stability, ease of synthesis and the ability to tune the plasmon resonance into the NIR are advantageous.[16] Altogether, these features make GNSs potent to thermally kill cancer cells when accumulated in the tumor tissue.[17,18] Nevertheless, therapeutic efficacy critically relies on the accumulation manner of those photothermal agents within the tumor tissue. Through intravenous administration, the accumulated amount of therapeutic agents is reduced due to the physiological barriers and imprecise targeting ability. Therefore, this systemic route requires high administration dose to achieve sufficient drug accumulation in the tumor.[19] Certainly, this is accompanied by harsh side effect and harm to the other healthy tissues.[20] Alternatively, intratumoral injection of the drug solution can be more efficient and lessen the required dosage. However, it might cause drug discharge to the surrounding healthy tissue, due to the limited space of the solid tumor interstitium, leading to toxicity risk and diminishing drug efficacy.[21]

MNs offer a minimally invasive method for precise localization of drugs in tissues. They are devices with needles of micrometer dimensions, capable of efficiently piercing through the stratum corneum barrier of skin, creating tiny channels for drug delivery into the viable tissue of skin.[22–24] Furthermore, MNs do not reach the deep dermis area in the skin that incorporate sensory nerve endings, making the drug delivery process painless.[25,26]

Dissolving MNs are made of water-soluble polymers such as polyvinyl alcohol (PVA), PVP and hyaluronic acid. They are easily applied, with fast dissolution in tissue to deliver the therapeutic cargo.[22,23,27] Despite the several types of MNs, e.g., solid and hollow MNs,[28] dissolving MNs are preferred for drug delivery due to their advantageous properties, e.g., reduced drug loss, high biocompatibility, enhanced drug availability and fast therapeutic release with no sharp and hazardous remaining waste.[29,30] Moreover, numerous studies have shown that dissolving MNs improve drug accumulation within the tumor tissue and provide uniform drug distribution,[23,31,32] making them potential candidates for transdermal delivery of therapeutics to superficial skin tumors.[21,33]

Thus, in the current study, we developed biocompatible PVP fast dissolving MNs incorporating GNS for PPT applications. The MNs are designed for efficient transdermal delivery, which will be optimal to target skin tumors, such as melanoma. Polyethylene glycol-modified GNSs were developed and loaded in dissolving PVP MNs. Next, GNSs were evaluated for their biocompatibility and their photothermal efficacy. Eventually, the developed GNSs-loaded MNs were further tested for their insertion ability and photothermal effect in excised porcine skin.

Table 1. The different GNSs formulations that were prepared, using two different concentrations of AgNO$_3$ (2 mM and 3 mM). In addition, in the table indicates whether PEG was added before or after the synthesis of the gold nanostars. The different formulas are denoted as F1 to F6.

Formulation	Concentration of AgNO$_3$	Order of PEG addition
F1	2 mM	during the synthesis of GNSs
F2	3 mM	
F3	2 mM	after the formation of GNSs and before centrifugation
F4	3 mM	
F5	2 mM	after the formation of GNSs and after centrifugation
F6	3 mM	

2. Experimental Section

Materials: Sodium citrate (MW = 294.10), ascorbic acid (MW = 176.12), silver nitrate (AgNO$_3$, MW = 169.87), Tetrachloroauric(III) acid trihydrate (HAuCl$_4$ · 3H$_2$O, MW 393.83), PEG 4000, PVP (K-90), and Parafilm were all purchased from Sigma-Aldrich, St. Louis, MO, USA. Dulbecco's Modified Eagle's medium (DMEM), fetal bovine serum, and penicillin/streptomycin were supplied by Fisher Scientific, Vantaa FINLAND. The luminescent cell viability assay (CellTiter-Glo) was purchased from Promega, Madison, Wisconsin, USA.

Preparation of PEG-Modified Gold Nanostars: Gold nanoparticles (GNPs) were first synthesized by reduction of gold ions using sodium citrate, followed by further reduction of silver ions using ascorbic acid to form gold nanostars. Briefly, 15 ml of Na citrate (1% w/v) was added to boiling 100 ml of 1 mM HAuCl$_4$. The mixture was stirred at 1000 rpm for 15 min and then let to cool down to room temperature. GNPs 100 µl was added to 10 ml of 0.25 mM of HAuCl$_4$ (0.1 mg ml^{-1}) and stirred at 700 rpm. A 100 µl of 2 or 3 mM AgNO3 was added to the mixture simultaneously with 50 µl of ascorbic acid (176 mg ml^{-1}) and stirred for 30 sec. This turns the color of the mixture instantly from a wine red color to a bluish color. PEG 4000 of 100 µl of 400 mg ml^{-1} either added during the synthesis mixed with GNPs and HAuCl$_4$ before adding AgNO$_3$ or added after the formation of GNSs and before/after centrifugation and stirred for 10 min as detailed in **Table 1**. The mixture was centrifuged at 5000 rpm for 15 min (Hettich EBA 21 Centrifuge, Marshall Scientific, Hampton, NH, USA) and the pellet was suspended in 0.5 ml of Milli-Q water. F1 and 3 needed higher speed of centrifugation to be separated from the dispersion (16 000 g for 15 min). The dispersions were washed and centrifuged, repeatedly, to purify the nanostars and ensure the removal of the reaction residual chemicals, e.g., silver ions and excess PEG. The pellet was finally dispersed in 0.5 ml Milli-Q water.

Characterization of Gold Nanostars: Plasmon resonance of the different GNSs was detected using a plate reader (Varioskan, Thermo Scientific, Waltham, MA, USA) at the wavelength range from 400–1000 nm, where each GNSs formulation was measured in triplicate (N = 3). Photothermal conversion studies were conducted for the GNSs in a 96 well-plate exposed to a laser (RLTMDL-808-2 W – diode laser system, Changchun New Industries Optoelectronics Tech. Co., Ltd. (CNI), Changchun, CHINA) of wavelength 808 nm and power 800 mW (Power supply: PSU-III-LED, Changchun New Industries Optoelectronics Tech. Co.,

**ADVANCED
SCIENCE NEWS**

www.advancedsciencenews.com

**ADVANCED
MATERIALS
TECHNOLOGIES**

www.advmattechnol.de

Ltd. (CNI), Changchun, CHINA) for 10 min, followed by imaging with a FLIR C2 Compact thermal camera (Teledyne FLIR LLC, Wilsonville, OR, USA). Thus, temperature change was monitored on the camera as well as the distribution and localization of the heat produced by GNSs. F2 and F4 were characterized for their average particle size (z-average), polydispersity index (PDI), and zeta-potential (ζ-potential) using a Malvern Zetasizer Nano instrument (Malvern Panalytical Ltd, Malvern, UK). Transmission electron microscopy (TEM) was used to study the morphology (Jeol JEM-1400, Jeol Ltd., Tokyo, Japan) of both F2 and F4. For this purpose, the particles were dispersed in water and then placed over copper-coated grids. The grids were dried at room temperature before imaging with TEM.

Cell Cytotoxicity: In order to evaluate the cytotoxicity of GNSs, the B16F10 cell line was used, a well-established melanoma cell line commonly used for toxicity studies. The cells were grown in DMEM supplemented with 10% of fetal bovine serum and 1% of penicillin/streptomycin in a humidified incubator at 37 °C with 5% CO_2. For the cytotoxicity assay, the B16F10 cells were incubated with increasing concentrations of GNSs, ranging from 1 to 100 µg ml^{-1}. Blank cell culture medium was used as control. After 24 h, the cell viability was measured using a CellTiterGlo luminescent assay and the luminescence obtained from a Varioskan LUX multimode microplate reader. All samples were tested in triplicates and the % cell viability was calculated.

In Vitro Photothermal Effect: B16F10 cells were seeded in a 96-well plate at a density of ≈15 000 cells per well one day prior to the experiment. The cell culture medium was replaced in each well with 200 µl of 25 µg ml^{-1} of GNSs (F4) versus treatment with blank culture medium (control). The cells were exposed to a NIR laser (808 nm) at 0.8 W cm^{-2} for 10 min. After the laser exposure, the cell viability was measured using a CellTiter-Glo luminescent assay and compared to the treated cells kept in the dark (non-irradiated). The luminescence intensity was obtained from a Varioskan LUX multimode microplate reader and % cell viability was calculated. All samples were tested in triplicate.

Fabrication the GNSs-Loaded MN: Dissolving MNs were fabricated using the micromolding method, wherein the polymer and GNSs suspension was casted into a negative mold and put to dry and solidify to form the MNs patch. MPatch Silicon negative molds were purchased (Micropoint Technologies PTE LTD, Singapore, SINGAPORE), comprising 10 × 10 MNs array. Each MN has a pyramidal shape with dimensions of height 800 µm, base 200 µm, and pitch 500 µm.

GNSs prepared in 100 ml solution were concentrated at a final volume of 250 µl of water for both types of GNSs (F2 and F4) and mixed with PVP 30% w/v in a ratio 1:1. The MNs were prepared according to the following protocol; 20 µL of GNSs-PVP mixture was added to the mold and centrifuged at 1000 × g for 10 min (Eppendorf Centrifuge 5810R, Eppendorf, Hamburg GERMANY), the excess suspension was removed using a spatula and then the MNs were let to dry in a vacuum oven for 30 min (400 mbar). The molding, centrifugation and drying steps were repeated 5 times to allow for enough concentration of the GNSs in the MNs. To form the base, 30 µL of PVP 30% w/v was added to the top of the MN mold and centrifuged at 180 g for 10 min followed by adding 100 µL of PVP 30% w/v and then let to dry in a desiccator at room temperature. Afterward, the MNs were demolded to be used in further experiments.

Characterization of Microneedles: *Photothermal Properties*: MNs were tested for their photothermal properties by exposure of the patches to a laser of 808 nm, 800 mW for 10 min. The patches were imaged by a thermal camera to detect the temperature of the patch.

Nanoparticles Re-Dispersibility: To check the re-dispersibility of the loaded GNSs, MNs of two patches were dissolved in 50 µl of water each and collected in an Eppendorf tube and 1 ml of water was added. The tube was centrifuged at 5000 rpm for 15 min. The pellet was dispersed in 1 ml water again to be centrifuged and washed again to be finally dispersed in 1 ml for TEM imaging.

Mechanical Properties: For fracture evaluation, MNs loaded with GNSs (F4) were fixed on the shaft of a Texture Analyzer (CT3, Brookfield, Massachusetts, USA) using a double-sided tape. The MNs were compressed against a metal surface by applying a force of 20N for 30 s with a speed of 0.5 mm s^{-1}. Afterward, the MNs were visualized under a light microscope to observe any changes in shape or integrity.

Penetration of MNs was evaluated using Parafilm as an elastic barrier. The MNs were placed on the top of the eight-layered Parafilm, and force was applied using a Texture Analyser (20N, for 30 s, with a speed of 0.5 mm s^{-1}). After that, the MNs and the parafilm layers were examined under light microscope. The number of MNs that penetrated each layer of Parafilm was counted and the penetration depth and efficiency were then calculated accordingly, provided that each MNs patch contained 100 MNs and the thickness of each Parafilm M layer was ≈127 µm.

Skin Insertion and Photothermal Effect of GNSs-Loaded MNs: Punches of 25 mm porcine skin were kept hydrated by putting over a pre-wetted filter paper in a petri dish. The skin surface was cleaned and dried using a tissue paper. the MNs loaded with GNSs (F4) was pressed by thumb on the skin surface for 3 min, left over the skin for 10 min and then the base of the MNs patch was further removed. The skin area containing the MNs was irradiated by 808 nm, 800 mW laser for 10 min. The skin was then imaged by a thermal camera to detect the temperature.

3. Results and Discussion

3.1. Preparation and Characterization of GNSs: PEG Functionalization and Plasmon resonance

GNSs were synthesized using the seed-mediated growth.[34] Thus, small GNPs were first formed as seeds, then GNSs were formed by mixing with $AgNO_3$, Ascorbic acid and $HAuCl_4$. Several studies have investigated the effect of $AgNO_3$ concentration on the synthesis of GNSs and their Plasmon resonance.[34,35] The results of these studies suggest that increasing the concentration of $AgNO_3$ leads to an increase in the size of the nanostars, as well as a red-shift in the Plasmon resonance peak.[35] Likewise, the morphology of the nanostars can also be affected by the $AgNO_3$ concentration, with higher concentrations leading to the formation of more star-like structures. Overall, the $AgNO_3$ concentration plays a crucial role in determining the properties of GNSs and their Plasmon resonance. Plasmon resonance is an important property of GNSs, which refers to the collective oscillation of conduction electrons on the surface of the nanoparticle, which can result in strong absorption of light.[36] The Plasmon resonance peak is the frequency at which the GNSs show the highest
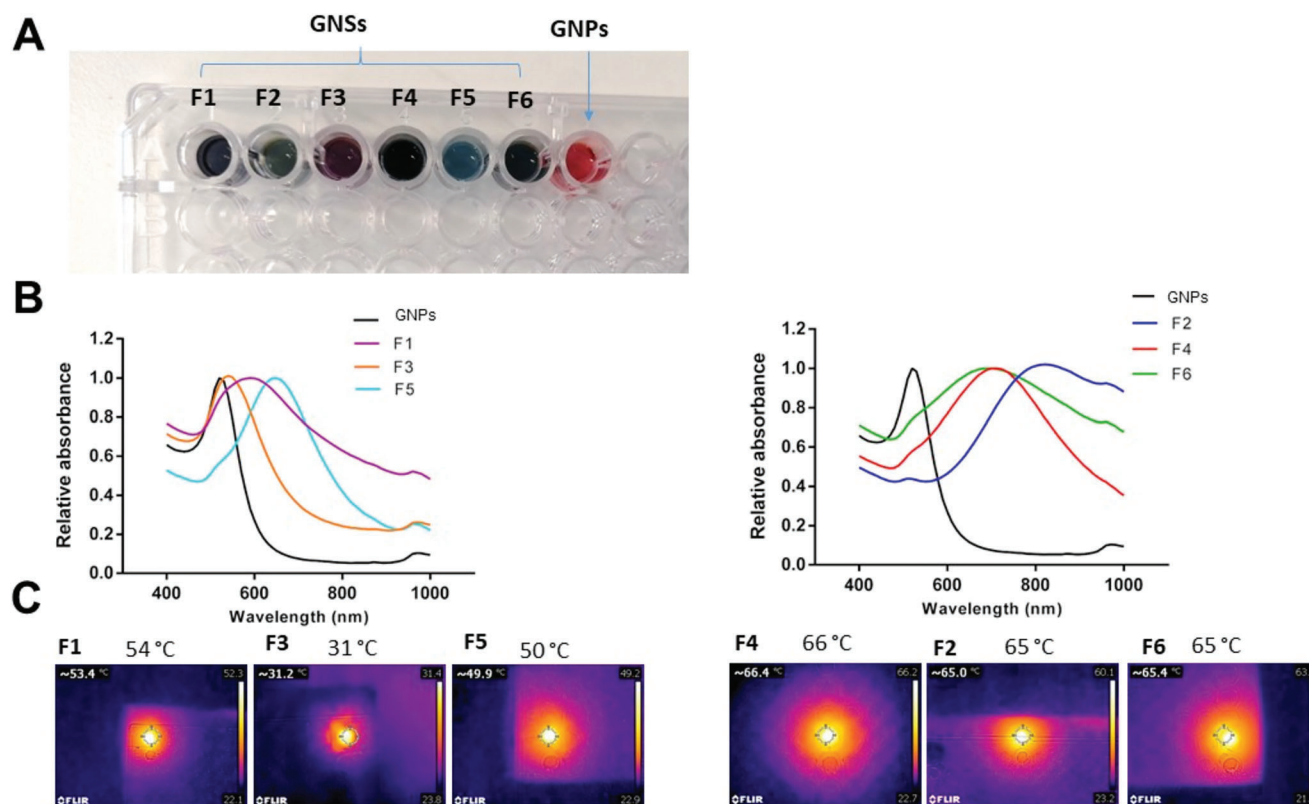
2301159 (3 of 9)

Figure 1. Different GNSs characterized for their Plasmon resonance and photothermal properties. A) Different GNS formulations mounted in 96-well plate showing different colors in comparison to gold nanoparticles. B) Spectral analysis of GNSs formulations using a microplate reader showing the peak of the highest absorption as the Plasmon resonance. C) Different GNSs formulations were exposed to NIR laser radiation (800 mW/10 min) and filmed by a thermal camera to measure the emitted heat. All measurements were performed in triplicate.

level of absorption and therefore heat generation, making it a useful parameter for assessing their potential for photothermal applications, such as cancer therapy, drug delivery, and photothermal imaging.[36] Several studies have also shown that hydrophilic polymers, e.g., PEG, exhibit a potential influence on the stability of nanoparticles.[37] Thus, PEG serves as a prominent non-ionic hydrophilic polymer for steric stabilization when adsorbed onto drug-delivery vehicles like gold nanostars.[38,39] This steric stabilization mechanism inhibits aggregation by creating a protective layer formed by PEG chains on the nanoparticle surface.[40] The repulsive forces among these chains prevent the close approximation of nanoparticles, enhancing formulation stability during storage and application.[41]

Beyond steric stabilization, the presence of PEG in the surrounding solution introduces a secondary, depletion stabilization mechanism. As gold nanostars come into proximity within the solution, the space between them becomes less favorable for the PEG chains, leading to a region of reduced PEG concentration known as the "polymer-depleted zone".[42] This depletion results in an osmotic pressure that generates repulsive forces, further preventing nanoparticle aggregation.[43,44]

Together, these dual stabilization mechanisms of PEG—steric and depletion—offer notable advantages over electrostatic stabilization, especially in environments with high ionic strength and in multiple phase systems.[45,46] The result is an enhanced dispersion and reduced agglomeration of nanoparticles.

Hence, in order to maximize the plasmon resonance of the fabricated GNSs, the preparation included experimenting adding two different concentrations of $AgNO_3$, 2 mM and 3 mM. Besides, the order of adding the stabilizing agent, PEG, were also varied. PEG was added in a different manner (Table 1, **Figure** 1A); during synthesis, after synthesis but before centrifugation or after synthesis and after centrifugation. The absorption spectra of these different formulas were recorded through UV–vis spectroscopy analysis and the peak corresponding to the plasmon resonance were identified. Besides, the synthesized nanoparticles were also characterized by TEM to examine their morphology.

The results suggest that the optimal $AgNO_3$ concentration was 3 mM as it resulted in higher Plasmon resonance 700–800 nm for the different formulations compared to the formulations that used 2 mM $AgNO_3$, which showed a Plasmon resonance ≈500 nm (Figure 1B). However, the order of adding PEG to the reaction seemed to be critical for the particles' Plasmon resonance. F2, where PEG was added during synthesis showed the second highest absorbance wavelength (690 nm), while F4 where PEG was added after synthesis but before centrifugation, showed the highest absorbance wavelength (800 nm) (Figure 1B). However, the F2 formula exhibited a broader absorbance peak > 800 nm. A broad peak of absorbance in Plasmon resonance typically means that the absorption is over a wide range of wavelengths and not confined to a narrow range of frequencies. This
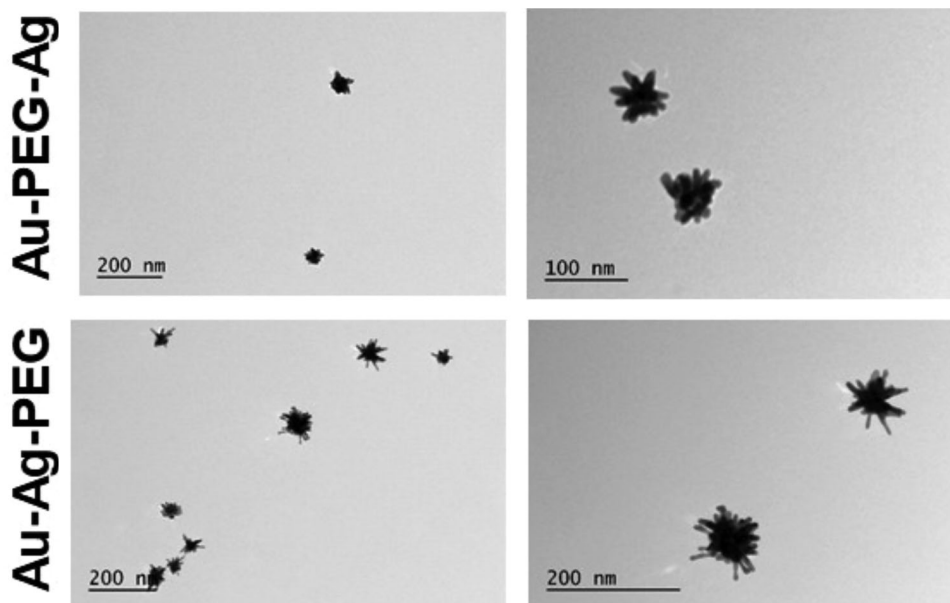
**ADVANCED
SCIENCE NEWS**

www.advancedsciencenews.com

**ADVANCED
MATERIALS
TECHNOLOGIES**

www.advmattechnol.de

Figure 2. TEM images of two different formulations of gold nanostars: F2 (Au-PEG-Ag) and F4 (Au-Ag-PEG).

may also indicate that the nanoparticles have a larger size distribution or that they have a more heterogeneous composition. A broad peak may also result from multiple peaks overlapping in the spectra.[38]

To assess the photothermal conversion efficiency of PEG-stabilized GNSs, two initial parameters were considered: (1) The maximum absorption wavelength and (2) the temperature generated upon irradiation. Hence, we subjected these formulations to NIR laser radiation, carefully capturing temperature variations using a thermal camera (Figure 1C).

Interestingly, despite the varied Plasmon resonance of F2 and F4, they both exhibited a similar photothermal effect when exposed to NIR laser (808 nm, 800 mW/10 min). Both formulas emitted heat equally, F2 (Au-PEG-Ag) ≈65 °C and F4 (Au-Ag-PEG) ≈66 °C (Figure 1C). TEM images of both formulations showed nicely formed star-shaped particles (**Figure 2**). Both showed closely similar size and zeta potential when measured by dynamic light scattering; Au-PEG-Ag (Size 74.53 ± 0.15 nm, PDI 0.24 ± 0.005, and zeta potential −28.83 ± 0.68 mV) and Au-Ag-PEG (Size 65.37 ± 0.50 nm, PDI 0.3 ± 0.004, and zeta potential −30.3 ± 0.9 mV).

The outcomes of this experimental setup obviously demonstrated the photothermal conversion efficiency of these PEG-stabilized GNSs. The observed temperature elevations stand as compelling evidence of their potential for effective photothermal applications. Guided by these promising results, and to validate the practical viability of our approach, we proceeded to address the cancer cell-killing effect and biocompatibility of these nanostars.

3.2. Cytotoxicity of GNSs

Several studies have demonstrated the safety and biocompatibility of both PVP polymer and gold nanostars when subjected to normal healthy cells.[47–49] Building upon this established knowl-

edge, our study is prospectively focused on evaluating the direct impact of our GNSs formulations on melanoma cell lines. The cytotoxicity of F2 (Au-PEG-Ag) and F4 (Au-Ag-PEG) on mouse melanoma cell line, B16F10, was investigated at different concentration of GNSs (from 1−100 µg ml^{-1}). Both F4 and F2 (**Figure 3**A) exhibit comparable cell viability, however, F4 showed slightly higher cell viability at higher concentrations (25–100 µg ml^{-1}). At concentration of 25 µg ml^{-1}, both formulations are biocompatible with cell viability > 80%. Our results support the findings of similar research, where PEGylated GNSs were proven nontoxic up to concentration of 20 µg ml^{-1}.[50] For further studies we have selected F2 (Au-PEG-Ag) due to the high Plasmon resonance wavelength (800 nm) (Figure 1A), which can allow the application of NIR laser with higher wavelength and thus increase the depth of light penetration in the tissue for in vivo applications. Subsequently, a concentration of 25 µg ml^{-1} of F2 (Au-PEG-Ag) was used to study the photo-cytotoxicity. The particles were incubated with B16F10 cells, and their cell viability was measured after NIR laser irradiation compared to non-irradiated cells (dark conditions). GNSs demonstrated instant high phototoxicity when exposed to the light (>90% toxicity). It is noteworthy that no visible aggregates of the nanostars was observed during the cytotoxicity studies, and the nanostars retained their photothermal efficiency, which might indicate the ability of PEG coating to maintain the stability of the nanostars in the cultural medium. This results clearly validate the photothermal effect of these GNSs and show their suitability to eradicate melanoma cancer cells due to the heat generated when exposed to NIR light (Figure 3B).

3.3. Preparation and Characterization of the GNSs-Loaded MNs

The MNs were successfully loaded with F2 (Au-PEG-Ag) as indicated with the dark blue color concentrated in the tips of the MNs
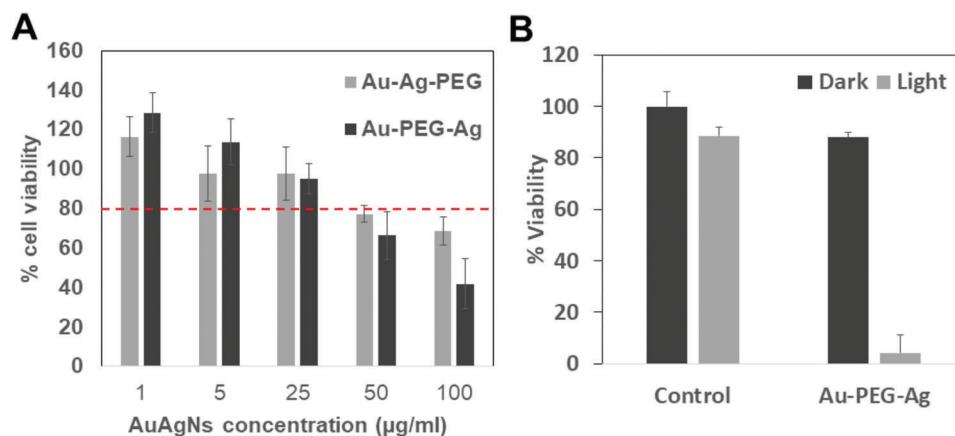
**ADVANCED
SCIENCE NEWS**

www.advancedsciencenews.com

**ADVANCED
MATERIALS
TECHNOLOGIES**

www.advmattechnol.de

Figure 3. A) Cell viability of B1610 melanoma cells treated with F2 (Au-PEG-Ag) and F4 (Au-Ag-PEG) against concentration range of 1–100 µg ml^{-1} using CellTiter-Glo assay, B) Instant cell killing of B16F10 cell line after addition of Au-PEG-Ag of 25 µg ml^{-1} concentration and irradiation by 808 nm laser of 0.8 mW cm^{-2} for 10 min against controls (untreated cells, untreated cell + irradiation, treated cells kept in the dark).

(**Figure 4**A). The MNs are pyramidal in shape arranged in 10×10 arrays in a 5×5 mm patches (Figure 4A; Figure S1, Supporting Information).

Characterizing F2 (Au-PEG-Ag) after dissolving the PVP MNs is crucial to assess the stability of the particles after loading in the MNs and to understand whether the MNs fabrication process and the drying has an effect on the stability of the released GNSs. TEM images of the released GNSs after MNs dissolution in PBS buffer, showed freely dispersed non-agglomerated star-shaped particles (Figure 4B). These results indicate that micromolding and dissolving MNs fabrication are suitable for deliv-

ering the GNSs, while maintain their stability. Additionally, the preservation of the star-like shape is significant because it is a key factor for the GNSs Plasmon resonance phenomena.[36] Further, the photothermal efficiency of F2 (Au-PEG-Ag)-loaded MNs were tested by irradiating the patches using 808 nm laser (800 mW for 10 min). The thermal imaging of the patch showed elevated temperature of 63 °C (Figure 4C), when the test was conducted at room temperature.

MNs are minimally invasive transdermal drug administration platform, which are proposed to replace the conventional hypodermic injections, due to several factors, e.g., painless
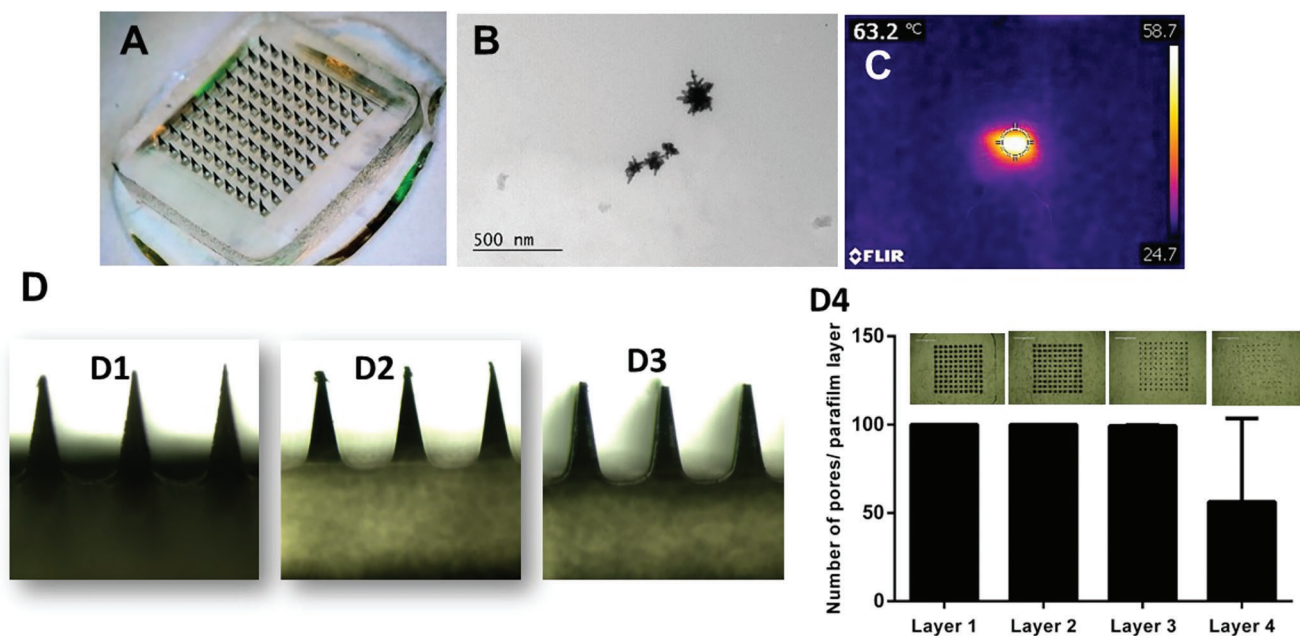

Figure 4. A) Magnified image of Au-PEG-Ag-loaded PVP microneedles, B) TEM image of the released Au-PEG-Ag, after dissolving the MNs, C) Thermal image of the microneedles patch after irradiation with 805 nm laser of 0.8 mW cm^{2-} for 10 min showing a rising temperature of ≈63 ° C,D) The mechanical properties of Au-PEG-Ag-loaded MNs; Insertion and fracture test. D1; Microscopical image of MNs as prepared, D2; Microscopical image of MNs after the fracture test, D3; Microscopical image of MNs after the insertion test in 8 layers of skin-simulant Parafilm, D4; The number of pores per layer of the Parafilm retrieved from the insertion test with inserted microscopical images of each layer.
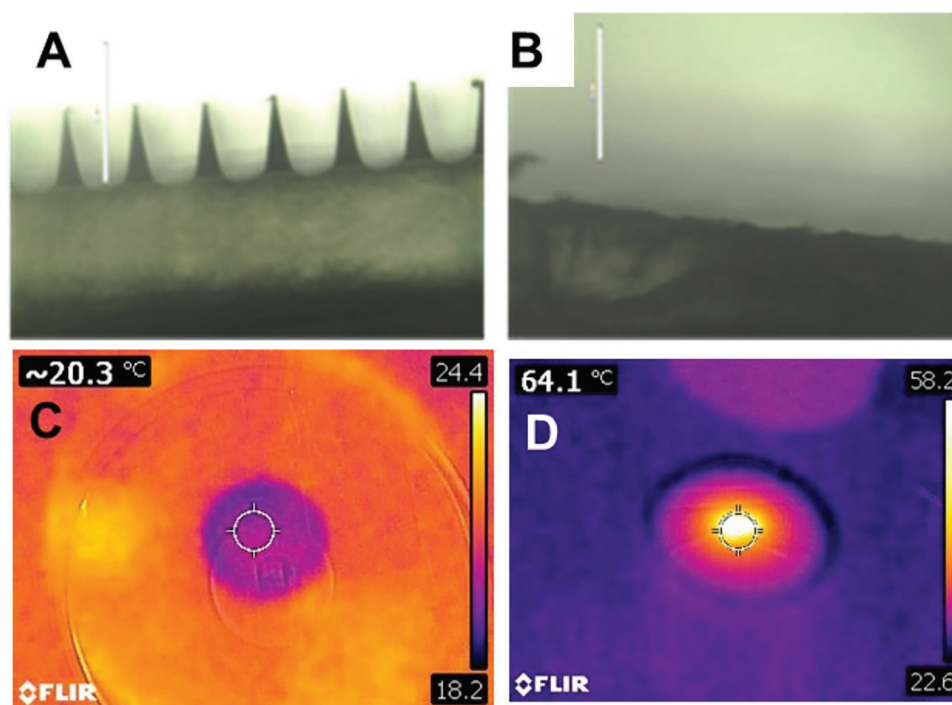
ADVANCED
SCIENCE NEWS
www.advancedsciencenews.com

ADVANCED
MATERIALS
TECHNOLOGIES
www.advmattechnol.de

Figure 5. A) Microscopic image of the microneedles before insertion in porcine skin, B) Microscopic image exhibits the complete dissolution of the microneedles after insertion into porcine skin for 3 min. C) Thermal image of porcine skin punch showing the skin temperature after insertion of Au-PEG-Ag-loaded PVP microneedles into porcine skin showing a temperature of ≈20° C. D) After irradiated with NIR laser the temperature rises to ≈64° C.

application and minimal hazardous waste. MNs open micropores in the skin layer (*Stratum corneum*), through which released therapeutic cargos can be delivered.[51] Thus, MNs patches must possess enough mechanical strength to penetrate the skin and overcome its inherent elasticity, which may otherwise cause deformation of the needles and result inadequate delivery. Hence, dissolvable F2 (Au-PEG-Au)-loaded MNs were characterized for their fracture resistance, as well as their ability to penetrate Parafilm-M layers.[52] Testing penetration ability of microneedles through parafilm is a method adopted originally from Larrañeta et al.,[53] where Parafilm was demonstrated as skin simulant suitable for comparative quality assessments and reliable insertion evaluation.

Fracture test was conducted to determine if the MNs of each patch will be able to penetrate the skin effectively and deliver the intended therapeutic payload without breaking or becoming deformed.[54] This is critical to assess the mechanical strength of the MNs, specifically their resistance to breaking or fracturing upon application to assure safe and convenient application. The test was done by applying a force on the patch and observing if the needles break or bend under the force. The applied force was 20N, which is the average force of human volunteers when applying MNs patches.[55] After applying the force on the patches for 30 sec, all the patches were examined under the light microscope to compare their integrity and deformation (Figure 4D1 before the test, and Figure 4D2 after the fracture test). The MNs remained intact with no deformation, showing sufficient mechanical strength to keep the integrity of the MN.

Insertion properties of those MNs were examined, wherein MNs patches were pressed against 8 layers of skin-simulant Parafilm (thickness ≈127 µm layer^{-1}). The microscopic examination of the MNs after Parafilm insertion revealed that MNs maintained their shape and only had a minimal number of fractured tips (Figure 4D3). Upon examining the film layers, it was found the MNs fully penetrated into the third layer of Parafilm, while 50% of MNs reached the fourth layer (a depth of penetration of 508 µm). This test simulates the insertion process of MNs into the skin and determines their effectiveness in delivering the photothermal load efficiently without breaking or bending. Altogether, the results from the fracture and piercing tests demonstrate the robust mechanical strength and effective piercing capability of PVP MNs.

3.3.1. Skin Penetration and Photothermal Effect of GNSs-Loaded MNs

F2 (Au-PEG-Ag)-loaded MNs showed efficient insertion in excised porcine skin and fast dissolution, both by manual application (using thumb pressure) and by using a texture analyzer with double-sided tape, as shown in the Supplementary Information (Video S1, Supporting Information). The base of the patch was removed after 3 min of insertion revealing a complete dissolution and separation of the MNs from the patch base as examined under light microscope. This is shown in **Figure 5**A; Figure S2 (Supporting Information), which showcase the MNs patch before insertion in skin, and in Figure 5B; Figure S3 (Supporting

Information), depicting the patch after insertion in skin. This rapid dissolution occurs due to the hydrophilic nature of the PVP polymer and good water solubility.[47]

The GNSs retained in skin, after MNs insertion and the patch base removal (Figure S4, Supporting Information), showing efficient photothermal activity when irradiated with NIR laser as recorded by a thermal camera. GNSs were able to absorb the light and generate heat ≈64 °C (Figure 5C,D). This outcome further proofs that microneedles do not hinder the release of gold nanostars, nor do they interfere with their dispersion state or photothermal characteristics. Moreover, the dispersed release of GNSs after dissolving the MNs, showed that PVP-polymer did not cause any aggregation of the GNSs nor affected their photothermal activity (Figure 4B).

Consequently, PVP MNs can act as an optimal platform to deliver GNSs into the skin while maintaining their photothermal activity. This represents a promising approach for pain-free administration of photothermal agents to deposit into local skin tumors, e.g., melanoma, for photothermal killing of cancer cells.

4. Conclusion

The combination of gold nanostars and microneedles offers a promising avenue for non-invasive and localized photothermal therapy in various skin conditions, especially melanoma. PEG-stabilized GNSs are developed and optimized to exhibit plasmon resonance in the NIR region. They are biocompatible and exhibit instant photothermal killing effect as tested in melanoma cancer cells B16F10. Furthermore, loading GNSs in MNs is a promising approach for painless delivery into skin. PVP-based MNs loaded with GNSs showed sufficient mechanical strength, rapid dissolution of the MNs, efficient skin insertion and photothermal efficiency.

The system exploits the high sensitivity of cancer cells to a raised temperature, thus facilitating targeted delivery of photothermal therapy. The system's adaptability for incorporating various therapeutic payloads, coupled with its ability to harness localized heat for treatment, opens doors for diverse applications beyond cancer therapy. The efficient and user-friendly delivery system aligns with the evolving landscape of patient-centered care, reflecting a shift towards minimally invasive treatments. However, further studies are necessary to evaluate the efficacy and safety of this system in treating skin cancers, such as melanoma.

Supporting Information

Supporting Information is available from the Wiley Online Library or from the author.

Acknowledgements

Conflict of Interest

The authors declare no conflict of interest.

Data Availability Statement

The data that support the findings of this study are available from the corresponding author upon reasonable request.

Keywords

[1] B. Ahmed, M. I. Qadir, S. Ghafoor, *Crit. Rev. Eukaryot. Gene Expr.* **2020**, *30*, 291.

[2] J. H. Kunishige, D. G. Brodland, J. A. Zitelli, *J. Am. Acad. Dermatol.* **2012**, *66*, 438.

[3] M. F. Simões, J. S. Sousa, A. C. Pais, *Cancer Lett.* **2015**, *357*, 8.

[4] S. J. Welsh, P. G. Corrie, *Ther. Adv. Med. Oncol.* **2015**, *7*, 122.

[5] S. A. Blankenstein, A. C. J. Van Akkooi, *Melanoma Res.* **2019**, *29*, 358.

[6] A. Mohammadpour, M. Derakhshan, H. Darabi, P. Hedayat, M. Momeni, *J. Cell. Physiol.* **2019**, *234*, 3307.

[7] L. Chablani, S. A. Tawde, A. Akalkotkar, M. J. D'souza, *AAPS J.* **2019**, *21*, PMID:30604321.

[8] Z. Yulin, C. Jiajie, T. Zhengfang, Z. Min, Z. Yufang, *J. Inorg. Mater.* **2020**, *35*, 1365.

[9] B. Zhao, Y.-Y. He, *Expert Rev. Anticancer Ther.* **2010**, *10*, 1797.

[10] Y. Mai, Z. Min, C. Yu, Z. Yufang, *J. Inorg. Mater.* **2021**, *36*, 1074.

[11] Y. Wang, W. You, X. Li, *Biocell* **2020**, *44*, 167.

[12] M. Chu, Y. Shao, J. Peng, X. Dai, H. Li, Q. Wu, D. Shi, *Biomaterials* **2013**, *34*, 4078.

[13] Z. Sobhani, M. A. Behnam, F. Emami, A. Dehghanian, I. Jamhiri, *Int. J. Nanomed.* **2017**, *12*, 4509.

[14] G. Guedes, S. Wang, F. Fontana, P. Figueiredo, J. Lindén, A. Correia, R. J. B. Pinto, S. Hietala, F. L. Sousa, H. A. Santos, *Adv. Mater.* **2021**, *33*, 2007761.

[15] X. Wang, G. Li, Y. Ding, S. Sun, *RSC Adv.* **2014**, *4*, 30375.

[16] Y. Wang, Y. Liu, H. Luehmann, X. Xia, P. Brown, C. Jarreau, M. Welch, Y. Xia, *ACS Nano* **2012**, *6*, 5880.

[17] F. Zhou, S. Wu, B. Wu, W. R. Chen, D. Xing, *Small* **2011**, *7*, 2727.

[18] E. Miyako, H. Kono, E. Yuba, C. Hosokawa, H. Nagai, Y. Hagihara, *Nat. Commun.* **2012**, *3*, PMID:23187626.

[19] D. Liu, D. T. Auguste, *J. Controlled Release* **2015**, *219*, 632.

[20] K. Hayashi, M. Nakamura, H. Miki, S. Ozaki, M. Abe, T. Matsumoto, W. Sakamoto, T. Yogo, K. Ishimura, *Theranostics* **2014**, *4*, 834.

[21] K. Ita, *Biomed. Pharmacother.* **2017**, *93*, 1116.

[22] T.-M. Tuan-Mahmood, M. T. C. Mccrudden, B. M. Torrisi, E. Mcalister, M. J. Garland, T. R. R. Singh, R. F. Donnelly, *Eur. J. Pharm. Sci.* **2013**, *50*, 623.

[23] M.-C. Chen, Z.-W. Lin, M.-H. Ling, *ACS Nano* **2016**, *10*, 93.

[24] H. Amani, M.-A. Shahbazi, C. D'Amico, F. Fontana, S. Abbaszadeh, H. A. Santos, *Drug Del.Trans. Res.* **2021**, *11*, 353.

[25] H. Amani, M.-A. Shahbazi, C. D'amico, F. Fontana, S. Abbaszadeh, H. A. Santos, *J. Controlled Release* **2021**, *330*, 185.

[26] T. Bauleth-Ramos, N. El-Sayed, F. Fontana, M. Lobita, M.-A. Shahbazi, H. A. Santos, *Mater. Today* **2023**, *63*, 239.

[27] B. Xu, Q. Cao, Y. Zhang, W. Yu, J. Zhu, D. Liu, G. Jiang, *ACS Biomater. Sci. Eng.* **2018**, *4*, 2473.

[28] N. S. Rejinold, J.-H. Shin, H. Y. Seok, Y.-C. Kim, *Expert Opin. Drug Deliv.* **2016**, *13*, 109.

[29] S. Hirobe, H. Azukizawa, T. Hanafusa, K. Matsuo, Y.-S. Quan, F. Kamiyama, I. Katayama, N. Okada, S. Nakagawa, *Biomaterials* **2015**, *57*, 50.

[30] Y.-H. Park, S. K. Ha, I. Choi, K. S. Kim, J. Park, N. Choi, B. Kim, J. H. Sung, *Biotechnol. Bioprocess Eng.* **2016**, *21*, 110.

[31] P. Pei, F. Yang, J. Liu, H. Hu, X. Du, N. Hanagata, S. Zhao, Y. Zhu, *Biomater. Sci.* **2018**, *6*, 1414.

[32] Y. Hao, Y. Chen, X. He, F. Yang, R. Han, C. Yang, W. Li, Z. Qian, *Bioact. Mater.* **2020**, *5*, 542.

[33] J. Arya, M. R. Prausnitz, *J. Controlled Release* **2016**, *240*, 135.

[34] Y. Li, J. Ma, Z. Ma, *Electrochim. Acta* **2013**, *108*, 435.

[35] D. Mulder, M. M. Phiri, B. C. Vorster, *Sens. Bio-Sens. Res.* **2019**, *25*, 100296.

[36] G. Chirico, M. Borzenkov, P. Pallavicini, in *Gold nanostars: synthesis, properties and biomedical application*, Springer, Berlin **2015**.

[37] K. Avgoustakis, *Curr. Drug Deliv.* **2004**, *1*, 321.

[38] K. Knop, R. Hoogenboom, D. Fischer, U. S. Schubert, *Angew. Chem., Int. Ed.* **2010**, *49*, 6288.

[39] J. Manson, D. Kumar, B. J. Meenan, D. Dixon, *Gold Bull.* **2011**, *44*, 99.

[40] G. F. De Lima, A. G. De Souza, D. S. Rosa, *J. Mol. Liq.* **2018**, *268*, 415.

[41] J. N. Israelachvili, in *Intermolecular and surface forces*, Academic press, Cambridge **2011**.

[42] T. Kuhl, Y. Guo, J. L. Alderfer, A. D. Berman, D. Leckband, J. Israelachvili, S. W. Hui, *Langmuir* **1996**, *12*, 3003.

[43] N. Biswas, M. Ichikawa, A. Datta, Y. T. Sato, M. Yanagisawa, K. Yoshikawa, *Chem. Phys. Lett.* **2012**, *539*, 157.

[44] K. Kim, S. Kim, J. Ryu, J. Jeon, S. G. Jang, H. Kim, D.-G. Gweon, W. B. Im, Y. Han, H. Kim, S. Q. Choi, *Nat. Commun.* **2017**, *8*, 14305.

[45] M.-C. Jones, J.-C. Leroux, *Eur. J. Pharm. Biopharm.* **1999**, *48*, 101.

[46] R. Ortiz, S. Olsen, E. Thormann, *Langmuir* **2018**, *34*, 4455.

[47] K. N. Mangang, P. Thakran, J. Halder, K. S. Yadav, G. Ghosh, D. Pradhan, G. Rath, V. K. Rai, *J. Biomater. Sci. Polym. Ed.* **2022**, *34*, PMID:36541167.

[48] P. M. Favi, M. Gao, L. Johana Sepúlveda Arango, S. P. Ospina, M. Morales, J. J. Pavon, T. J. Webster, *J. Biomed. Mater. Res., Part A* **2015**, *103*, 3449.

[49] M. Bhamidipati, L. Fabris, *Bioconjugate Chem.* **2017**, *28*, 449.

[50] X. Xie, J. Liao, X. Shao, Q. Li, Y. Lin, *Sci. Rep.* **2017**, *7*, 3827.

[51] J. S. Kochhar, T. C. Quek, W. J. Soon, J. Choi, S. Zou, L. Kang, *J. Pharm. Sci.* **2013**, *102*, 4100.

[52] S. Rojekar, L. K. Vora, I. A. Tekko, F. Volpe-Zanutto, H. O. Mccarthy, P. R. Vavia, R. F. Donnelly, *Eur. J. Pharm. Biopharm.* **2021**, *165*, 41.

[53] E. Larrañeta, J. Moore, E. M. Vicente-Pérez, P. González-Vázquez, R. Lutton, A. D. Woolfson, R. F. Donnelly, *Int. J. Pharm.* **2014**, *472*, 65.

[54] P. Khanna, B. R. Flam, B. Osborn, J. A. Strom, S. Bhansali, *Sens. Actuators, A* **2011**, *170*, 180.

[55] A. Ripolin, J. Quinn, E. Larrañeta, E. M. Vicente-Perez, J. Barry, R. F. Donnelly, *Int. J. Pharmaceut.* **2017**, *521*, 92.